Influence of Machine Integration on the Thermal Behavior of a PM Drive for Hybrid Electric Traction

Christian Paar
Projecthouse EU
Magna Powertrain AG & Co KG
8200 Albersdorf, Austria
Email: christian.paar@magnapowertrain.com

Hendrik Kolbe and Annette Muetze
Electric Drives and Machines Institute
University of Technology
8010 Graz, Austria
Email: hendrik.kolbe@tugraz.at, muetze@tugraz.at

***Abstract*—We present a method for fast identification of the thermal behavior of vehicle integrated electric drives to propose a better understanding of electric machine design tailored to driving cycles. A simple, but satisfactorily accurate calculation method for the estimation of machine losses, which is an input for the analytic thermal network, in the early design stage is introduced. The analytic models, which are verified using measurement data, are used for parameter and case studies for consideration of the thermal environment with focus on the gearbox. An improvement of machine performance using an alternative cooling approach which cools down the end windings is shown in the final section of the paper.**

I. Motivation

A key design issue of electric drives for hybrid electric vehicles is the trade-off between power density and performance. A special design challenge of drives for such applications is given by the driving profiles that can hardly be described by the definition of a rated torque and speed, the parameters electric machines have been specified with for decades. The correlations between the electromagnetic design of electric machines and their cooling types have been investigated for a long time. Current approaches during the conceptual design and development phase typically meet the manifold torque-speed requirements by e.g. oversizing of the drive (reduced shear force density and current sheet loading) [1] to exploit the thermal inertia for short term overload operation and/or use costly high temperature performance materials like dysprosium [2]. Another approach to achieve packaging targets is the use of high performance sheets (Fe-Co) to increase the possible air gap flux density [3], which also comes at the disadvantage of a higher price. Specific thermal optimization of the electric drive considering its thermal environment and operating profile allows better meeting of customer requirements like packaging, weight, performance, and costs. This thermal environment considers the mounting of the machine and thereby allows for exploitation of already existing thermal paths. The results we present aim to contribute to a better understanding of electric machine design tailored to the driving cycles and the thermal environment as they occur with electric traction operation. Such work requires the availability of a fast design process to enable a quick identification of thermal paths in the drive and at relevant mounting points. The chosen analytic modeling approach will be presented first. Then, the influences of additional heat sources/sinks as they may occur with highly integrated drives, such as electric clutch systems and gearboxes (for gearbox integrated drives) are studied. The electric machine for the studies in this publication is a 50 kW peak power and 20 kW continuous power interior mounted permanent magnet synchronous electric machine (IPM) with water jacket cooling. The IPM has a peak torque of 200 Nm during overload operation.

II. Modeling Approach

A. Analytic Loss Model

To ensure fast parameter studies, an analytic approach is considered appropriate. The following loss sources are modeled:

1. Winding Copper Losses (Joule Losses)

$$P_{\mathrm{CU}} = m\, I_{\mathrm{ph}}^2 R\left(\theta\right) k_{\mathrm{s}}\,, \tag{1}$$

where m is the number of phases, I_{ph} is the phase current and $R\left(\theta\right)$ the phase resistance which depends on temperature θ. Skin and proximity losses are considered by the correction factor k_s [4].

2. Iron Losses

For a fast computation of the iron losses in the different parts of the machine (core backs and teeth), the established Steinmetz equation [5] is used,

$$P_{\mathrm{fe}} = m\, p_{\mathrm{fe}} \left(\frac{B}{B_{\mathrm{ref}}}\right)^2 \left(\frac{f}{f_{\mathrm{ref}}}\right)^{1.6} k_{\mathrm{p}}\,, \tag{2}$$

with flux density B, reference flux density B_{ref}, frequency f, reference frequency f_{ref}, where the factor k_{p} considers the degradation of the magnetic properties of the lamination material due to manufacturing. The modeling depth of the magnetic circuit for the calculation of the flux densities is determined by the geometric complexity of the flux paths.

978-1-4799-5776-7/14/$31.00 ©2014 IEEE

An appropriate calculation approach for the estimation of the machine losses is an equivalent circuit model similar to the one presented in [6], which describes the magnetic circuit by stator back iron, teeth, airgap, rotor yoke, and permanent magnet equivalent reluctance.

3. Additional Losses

For example, the eddy and hysteresis losses in the magnets [6] are estimated according to [7],

$$P_{\mathrm{add}} = C_{\mathrm{add}} \left(\frac{I_{\mathrm{ph}}}{I_{\mathrm{ph,n}}} \right)^2 \left(\frac{f}{f_{\mathrm{n}}} \right)^{1.6} P_{\mathrm{n}} \,, \tag{3}$$

where the additional loss factor C_{add} is approximately 0.0075, P_{n} is the nominal power, f_{n} is the nominal frequency and $I_{\mathrm{ph,n}}$ is the nominal phase current. FEM simulations of the realized machine showed that these losses are at approximately 1% of the total losses.

4. Windage Losses

The mechanical losses caused by air friction (windage losses) are modeled according to [7],

$$P_{\mathrm{m,air}} = C_{\mathrm{m}} v^2 d_{\mathrm{R}} l_{\mathrm{fe}} \,, \tag{4}$$

where v is the surface speed, d_{R} is the rotor diameter and l_{fe} is the stack length. The empirical value C_{m} is assumed at $8 - 10$ for surface aeration and up to 15 for internal cooling [7].

5. Gearbox and External Losses

The losses which occur within the gearbox and those introduced into the system from additional loss sources (e.g. sealing rings) are based on measurements. Especially the sealing ring losses, windage losses and bearing losses need special consideration as they occur on distributed locations within the drive and affect the loss distribution in the analytic model. Therefore, we investigated these losses on a test bench with a dummy rotor (to avoid cogging torque). The measurements were carried out at different temperatures (from $-25\,^{\circ}\mathrm{C}$ up to $120\,^{\circ}\mathrm{C}$). The second step was the repetition of the test program with the seal rings removed. The third and the last step was its repetition with the seal rings and the rotor removed.

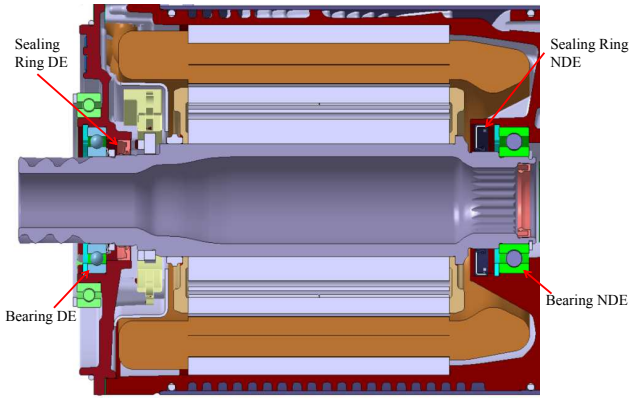

Fig. 1. Electric drive cross section view, with location of bearings and sealing rings at NDE and DE.

These measurements allow a seperation of the gearbox, seal rings, windage and bearing losses at the drive-end (DE) and nondrive-end (NDE) (Fig.1).

B. Thermal Model

The Finite-Element-Method (FEM) and/or Computational-Fluid-Dynamics (CFD) in combination with measurement data are used to determine selected heat transfer parameters (especially if using a liquid or air cooled system), for the thermal model. As with the electromagnetic design, both analytic lumped circuit and numerical methods are available [8]. Both approaches require the definition of the thermal parameters, which is a complex task because of the complex materials and material combinations such as the laminated steel, impregnated wires or wires with dual coating. Furthermore, not only thermal conduction occurs within the drive, but also free and forced convections and radiation. In addition, different types of cooling may be required to be investigated and compared.

Here again, the approach of a lumped analytic model is taken, with certain parameters determined through numerical methods, measurements and literature [9], [10]. This allows determining the temperatures at selected points, such as the coolant temperature at the outer perimeter of the machine or the temperature in the center point of the magnets. The exact temperature distributions within certain parts of the machine, such as the magnets, cannot be computed with this approach, which is acceptable considering the focus of the presented work.

The lumped parameter model developed for this study (Fig. 2, baseline case) is designed to calculate the temperature at the following nodes: 0 - node of average coolant temperature, 1 - cooling jacket node, 2 - point of average stator yoke temperature, 3 - point of average teeth temperature, 4 - boundary between stator teeth and air gap, 5 - boundary between air gap and rotor surface, 6 - virtual average rotor point, 7 - virtual midpoint of bearing at NDE, 8 - virtual midpoint of bearing at DE, 9 - point of average winding temperature in stator slots, 10 - point of average temperature of end winding (overhang) at NDE, 11 - point of average temperature of end winding at DE, 12 - point of average shaft surface temperature, 13 - virtual point within frame between equivalent axial and radial section at NDE, 14 - virtual point within frame between equivalent axial and radial section at DE, 15 - virtual point in air volume in end winding region at NDE, 16 - virtual point in air volume in end winding region at DE, 17 - virtual point of average side surface temperature of rotor at NDE, 18 - virtual point of average side surface temperature of rotor at DE, 19 - virtual point of average surface temperature of end winding at NDE, 20 - virtual point of average surface temperature of end winding at DE.

The following thermal capacities are modeled: C_1 - thermal capacity of the frame (and mounted parts), C_2 - stator yoke, C_3 - stator teeth, C_6 - rotor, C_7/C_8 - bearings, C_9 - slots, C_{10} - end winding at NDE, C_{11} - end winding at DE, C_{12} - shaft, C_{15} inner air at DE, C_{16} - inner air at DE.

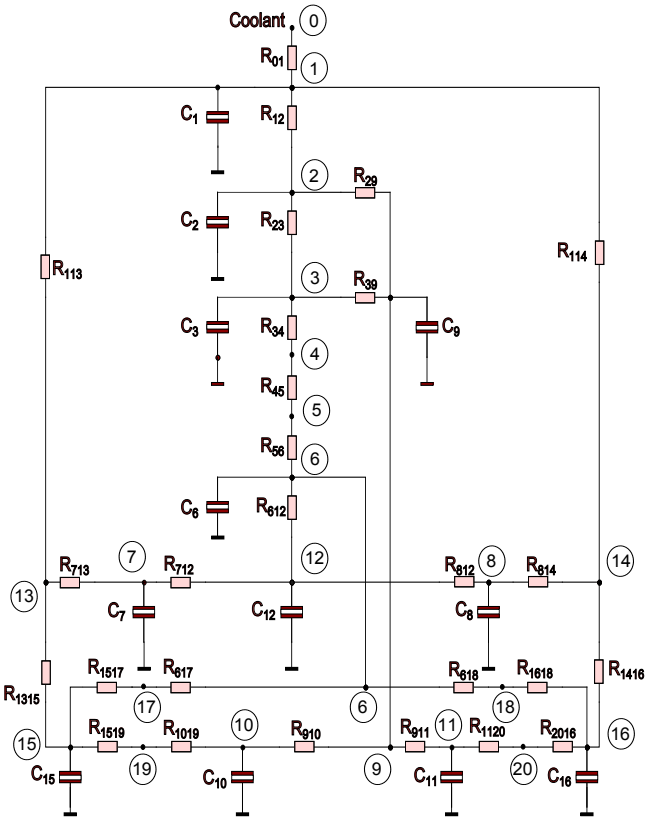

Fig. 2. Thermal lumped parameter model.

This lumped parameter model may be summarised mathematically as

$$\underline{C}\frac{d\vec{\theta}\,(t)}{dt} = \vec{P} - \underline{G}\vec{\theta}\,(t)\ , \tag{5}$$

with the vector of loss injections $\vec{P}$, the conductivity matrix $\underline{G}$, the temperature vector

$$\vec{\theta}\,(t) = \begin{pmatrix} \theta_1(t) \\ \theta_2(t) \\ \theta_3(t) \\ \vdots \\ \theta_i(t) \end{pmatrix} \tag{6}$$

and the diagonal matrix $\underline{C}$ which defines the capacity for each node as indicated in Fig. 2. The model is solved in MATLAB/Simulink.

The thermal conductivities in the matrix $\underline{G}$ are series and parallel resistances of equivalent thermal resistances defined by contact resistance, convection and radiation. The contact and/or convection conductance is defined as

$$G = h\,A, \tag{7}$$

with surface area A and the effective contact or convection heat transfer coefficient h. This thermal lumped parameter model assumes that the heat transfer in the radial and axial directions can be treated independently from each other [10]. As a direct consequence, different heat flow paths, for instance heat flow in axial and radial direction, can be treated as problems related to one-dimensional heat transfer. Of critical importance is the correct connection of the different paths, i.e. the thermal resistances, thermal capacitances and power injections of the corresponding element in the lumped parameter model.

C. Vehicle Model and Driving Cycles

Relevant driving cycles for governmental emission homologation of vehicles are the New European Driving Cycle (NEDC) for the EU and the Federal Test Procedure (FTP-75) for the United States. The fuel and emission regulations depend on national legislations [11], [12]. Furthermore, in future (as proposed by the EU-parliament) the Worldwide Harmonized Light Vehicles Test Procedure (WLTP) may be relevant [11]. In this publication the FTP-75 (Fig. 3) was considered, because it requires higher torque dynamics to fulfill the speed target over time, when compared to the NEDC.

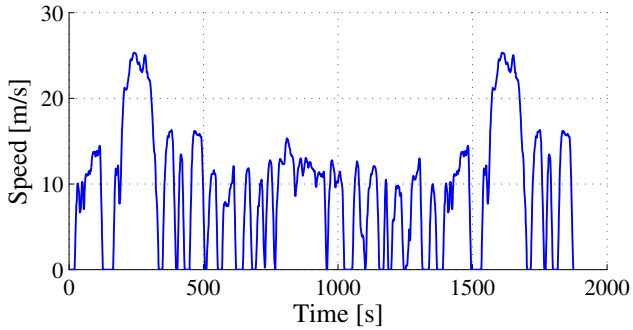

Fig. 3. FTP-75 speed profile.

For the calculation of the electric drive torque profile a simple longitudinal vehicle model using a quasi-static approach was used [13]. The quasi-static vehicle model calculates the torque profile for the electric drive from a given speed profile without considering dynamic effects in the vehicle drive train. Focusing on the electric drive, no hybrid vehicle control strategies were considered. The mid-size car simulated has a curb weight of $m_\mathrm{c} = 2058\,\mathrm{kg}$. A load (driver) weight of $m_\mathrm{l} = 75\,\mathrm{kg}$ was assumed for the simulations to calculate the total driving force

$$F_\mathrm{v} = m_\mathrm{v} g \mu_\mathrm{r} + \frac{A_\mathrm{v} v_\mathrm{v}^2 \rho c_\mathrm{w}}{2} + (m_\mathrm{C} f_\mathrm{rot} + m_\mathrm{l})\,\dot{v}_\mathrm{v}\,, \tag{8}$$

with vehicle speed v_v, air density ρ, total vehicle weight $m_\mathrm{v} = m_\mathrm{c} + m_\mathrm{l}$ and force of gravity $g = 9.81\,\frac{\mathrm{m}}{\mathrm{s}^2}$. The rolling friction constant, which depends on the road surface wheel contact, was assumed with $\mu_\mathrm{r} = 0.008$. The vehicle cross sectional area is $A_\mathrm{v} = 2.28\,\mathrm{m}$ with a drag coefficient $c_\mathrm{w} = 0.29$. The factor f_rot is a simplification to consider the rotational masses (inertia) of the drive train as a percentage share of the curb weight, and was estimated with $5\,\%$ of the curb weight ($f_\mathrm{rot} = 1.05$). The total force is used to calculate the current shaft torque of the electric drive using the tire radius. The gearbox losses are implemented using a look up table which is based on experimental results.

III. Model Validation

A. Validation of Loss Model

For the validation of the loss model, measurements are used to verify the overall model accuracy. Table I depicts the results for selected operating points. They illustrate the overall model accuracy in a wide torque and speed range. The proposed analytic approach shows a sufficient agreement with measured data and FEM model results.

TABLE I
COMPARISON OF TOTAL LOSSES: FEM, LOSS MODEL AND MEASUREMENT RESULT DATA

	FEM	Meas.	Model	Difference Model & Meas.
250 rpm 200 Nm	5741 W	5933 W	5706 W	−3.83 %
2000 rpm 200 Nm	6245 W	6327 W	6073 W	−4.00 %
4000 rpm 60 Nm	1130 W	1138 W	1167 W	−2.55 %
7000 rpm 20 Nm	917 W	918 W	906 W	−1.27 %
11000 rpm 20 Nm	2107 W	2073 W	1916 W	−8.20 %

To ensure accurate results of the temperature model, the loss distribution in the electric drive must also be regarded. The loss deviation for the mechanical losses was determined using the test-rig (Fig. 5). The proportional distribution of the iron losses is not discussed in detail at this point, because the accuracy is also reflected by the temperatures. The temperature model with measured temperatures is discussed in the following section.

B. Validation of Temperature Model

Table II compares the measured data and the analytic simulation results for four different operating points (steady state). Relevant points are the DE and NDE end winding, the winding temperature in the slots, and the rotor (respectively magnet) temperature. Note that these results already indicate the important role of the end windings both at the NDE and at the DE of the machine, these are the machine hotspots.

TABLE II
CHARACTERISTIC DRIVE TEMPERATURES AT DIFFERENT OPERATING POINTS

	1000 rpm, 90 Nm		2150 rpm, 90 Nm	
	Meas.	Model	Meas.	Model
Winding, slot	118.0 °C	116.4 °C	123.5 °C	116.1 °C
Winding, NDE	113.9 °C	126.0 °C	117.6 °C	124.8 °C
Winding, DE	126.6 °C	126.1 °C	132.5 °C	124.7 °C
Coolant outlet	69.7 °C	70.1 °C	70.5 °C	70.2 °C
Rotor	71.4 °C	97.4 °C	77.9 °C	95.5 °C
	6000 rpm, 32 Nm		12000 rpm, 17 Nm	
	Meas.	Model	Meas.	Model
Winding, slot	88.6 °C	81.4 °C	111.6 °C	99.6 °C
Winding, NDE	85.5 °C	82.4 °C	103.7 °C	99.9 °C
Winding, DE	89.3 °C	82.6 °C	112.4 °C	100.5 °C
Coolant outlet	67.0 °C	66.6 °C	69.6 °C	69.1 °C
Rotor	74.8 °C	82.6 °C	88.4 °C	105.5 °C

The modeled rotor temperature is higher than the one measured (Tab. II). As the bearings are lubricated by the attached gearbox through special oil ducts, the test-rig was set up to ensure a defined lubrication of the bearings with 39 $\frac{\text{ml}}{\text{min}}$ lube supply for each bearing using lubrication tubes (Fig. 5). The temperature of the oil sump was measured. From the change of temperature out of the bearings, a negative heat flow was determined (nodes 7 and 8 in Fig. 2). However, this defined lubrication flow does not correspond to the lubrication situation with the gearbox attached, therefore this difference between measured and modeled rotor temperature is acceptable.

Fig. 4 shows the behavior under dynamic condition, to represent the transient validation. The electric drive was warmed up at 90 Nm and 1000 rpm until the end winding temperatures had reached a steady state temperature of 120 °C, after that a 200 Nm peak torque step at 2380 rpm was applied for 30 s.

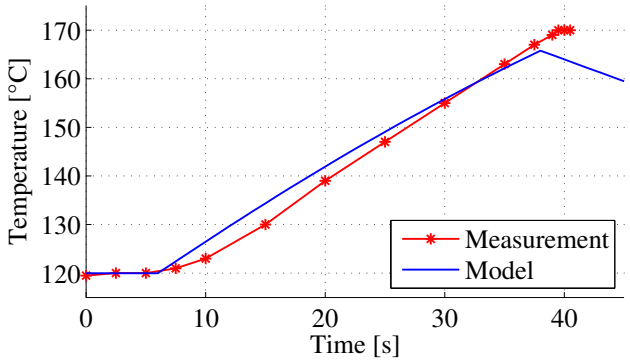

Fig. 4. End winding temperature DE: thermal transient 30 s peak torque step response at 2380 rpm.

The step response in Fig. 4 indicates a sufficient accuracy of the thermal time constants as well as determined thermal capacities in the model.

Fig. 5. Test rig with thermal insulation box and lubrication tubes.

IV. Integration Study

Aiming to study the thermal effects of drive integration in the vehicle environment, we investigate the influences of a gearbox mounted onto the machine, for different coolant temperatures and alternative cooling methods. Subsection IV-A discusses the influence of the gearbox on the end winding and magnet center temperatures, while Subsection IV-B considers the influence and capability of additional oil spray cooling of end windings.

A. Case 1: Gearbox Integration

We consider a water cooled machine similar to the one the model was experimentally validated with. An additional gearbox is mounted at its DE. Starting from a no load operating point at 2150 rpm and a gearbox temperature of 80 °C a boost cycle with 200 Nm for 25 s is applied. Then, the gearbox contributes an additional 520 W losses (interpolated from mechanical measurements at 2150 rpm, spin and load depending losses) which is 10 % of the total machine losses in this operating point. For calculation of the steady state operating point, the spin losses of the gearbox were considered, during the boost cycle also the additional load-dependent losses were taken into account. The computed end winding and magnet temperatures are shown in Fig. 6, with the end winding surface temperatures and the magnet temperatures.

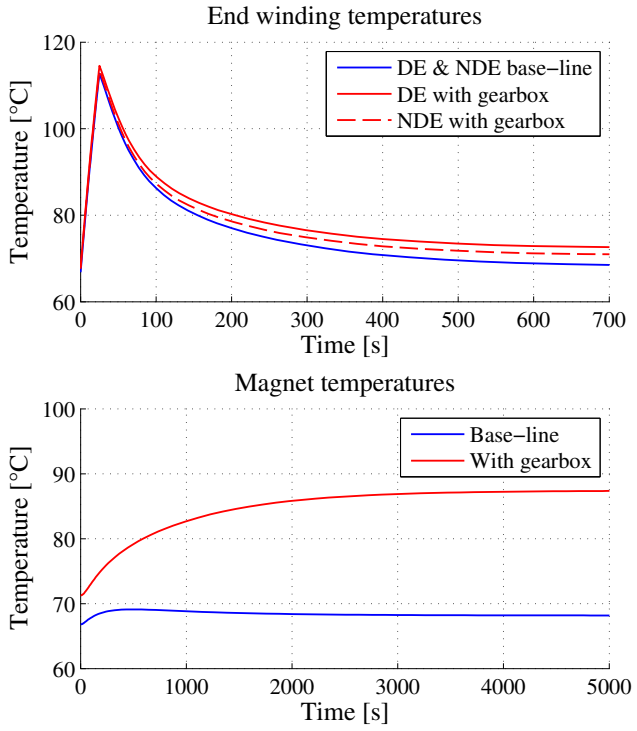

Fig. 6. Comparison: influence of gearbox losses for end winding and magnet temperatures for a 25 s boost cycle.

Under these conditions, the average end winding temperature of both sides reaches a maximum of 114 °C (NDE-DE difference: 1 K) after 25 s. This is only 1.3 K higher than the mean winding temperature without consideration of the gearbox (base-line). The end winding initial temperature without the gearbox is 67 °C and is defined by the cooling temperature. The mean initial temperature with the gearbox attached is only 1 K higher and the temperature difference between the two sides of the drive is 3 K. Thus, for this specific drive, the additional heat introduced by the gear box losses does not affect the end winding temperature, significantly.

The situation is, however, very different for the magnets: the additional heat flow from the rotor due to the gear box increases the temperature of the magnets by 19 K (Fig. 6). This may, in turn, severely impede the performance of the motor, as the magnets may provide less magnetic flux, and more phase current might be required for the desired torque to be produced, increasing the losses and thus the heat development further. For example, a 10 % decrease in magnetic flux would need to be compensated by a 10 % increase of armature current, assuming linear behaviour. This, in turn, would result in a 21 % increase of the copper losses.

To evaluate the relevancy of the gearbox influence on the rotor temperature during a driving cycle, the specified setup was simulated with and without the gearbox using the vehicle model introduced in Section II-C. Fig. 7 indicates the important role of the gearbox losses if focusing on the magnet (rotor) temperature respectively. The magnet temperature after the cycle is 7 K higher if gearbox losses are considered. However, the temperature remains below the critical limits.

B. Case 2: Alternative Cooling Method

Next, the influence of oil-cooled end windings (splash-oil cooling) was studied. The heat transfer coefficients were taken from literature [14]. The heat transfer coefficient between the oil (automatic transmission fluid, ATF) and the end-winding is a nonlinear function of the temperature [14]. For the range of temperatures occurring within this study, it varies between 100 $\frac{\mathrm{W}}{\mathrm{m^2K}}$ and 300 $\frac{\mathrm{W}}{\mathrm{m^2K}}$. As in the previous case a 25 s torque step, starting from the nominal operating point at steady state, is applied. An oil spray temperature (ATF as cooling fluid)

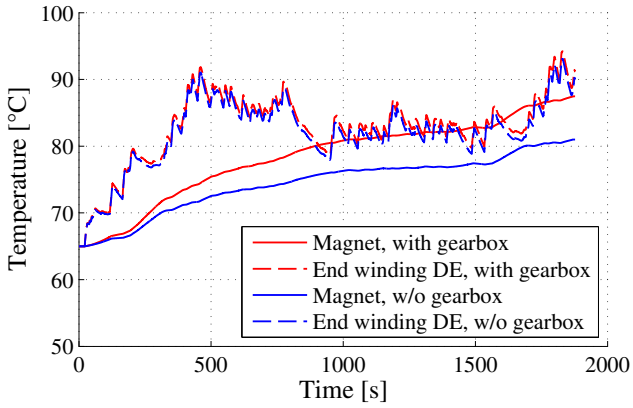

Fig. 7. Comparison: magnet and end winding temperatures at DE with and without consideration of gearbox.

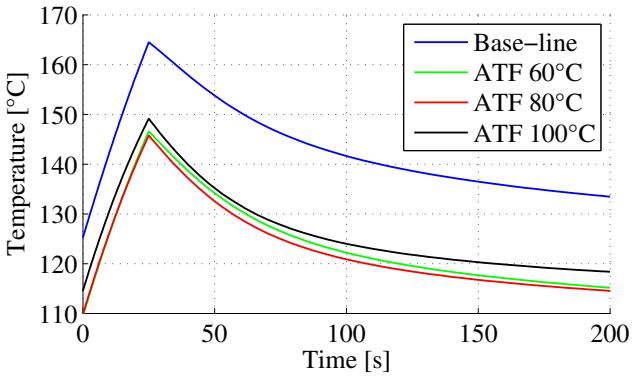

Fig. 8. Comparison of end winding temperatures during boost cycle.

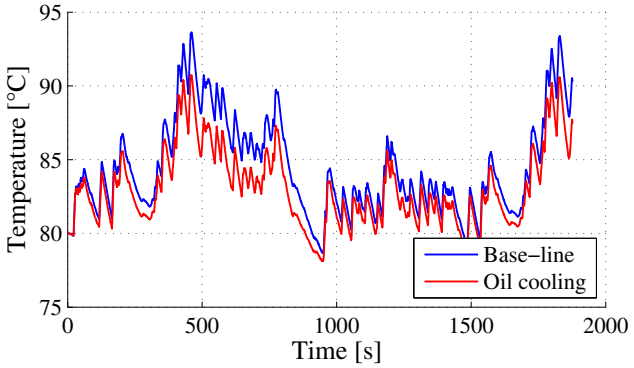

Fig. 9. Comparison: magnet temperatures with and without oil cooling.

of 80 °C decreases the temperature of the end winding by 19 K, from 165 °C down to 146 °C, that of the winding in the slots only by 6 K, from 147 °C down to 138 °C. Fig. 8 shows the difference between the base-line case (no gearbox, no oil-spray cooling on end winding) and the effect of oil-spray cooling for different ATF temperatures. The increasing heat transfer coefficient with increasing cooling fluid temperatures may suggest that the largest effect would be obtained at high oil temperatures. However, high cooling fluid temperatures heat up the system. Therefore the largest cooling effort can be obtained for a fluid temperature of 80 °C. This point is the best compromise between fluid temperature and heat transfer coefficient.

To conclude the study, the drive performance with ATF cooling at 80 °C was simulated for the FTP-75 driving cycle (Fig. 9). The cooling improvement was emphasized.

V. Conclusion

The possible influences of a gearbox and oil-spray cooling on the thermal behavior of an IPM machine for electric traction applications are studied. To this aim, a fast analytic approach has been developed that draws from a model that had been validated experimentally. The vehicle model follows a quasi-static approach to speed up the simulation and allow for future parameter studies. Aiming to study the thermal effects of drive integration in a vehicle environment, we investigate the influences of an additional gearbox mounted onto the machine in the first case study. The studies illustrate the role of the drive integration for thermal studies of electric drives, notably the consideration of additional heat sinks/sources exterior to the main machine. The case studies borrow from drives as they have been realized. The effort of the direct winding overhang-cooling was shown and applied to a real world driving cycle in the second case study.

Acknowledgment

The paper presented is gratefully supported by the Austrian Research Promotion Agency (FFG) and the Styrian Business Promotion Agency (SFG). Further gratitude is to conveyed to the Austrian Government and Province of Styria as proprietary of the respectively promotional agencies.

References

[1] C. M. Liao, C. L. Chen, and T. Katcher, "Thermal analysis for design of high performance motors," in *Thermal and Thermomechanical Phenomena in Electronic Systems, 1998. ITHERM '98. The Sixth Intersociety Conference on*, 1998, pp. 424–433, iD: 1.

[2] K. Bennion. (2013) Electric motor thermal management. Accessed on 2014-01-13. [Online]. Available: http://www4.eere.energy.gov/vehiclesandfuels/resources/merit-review/sites/default/files/ape030_bennion_2013_o.pdf

[3] I. Adcock, "Winning the power struggle," *Automotivedesign*, no. March/April, pp. 12–15, 2012.

[4] G. Mueller, K. Vogt, and B. Ponick, *Berechnung elektrischer Maschinen, 6., voellig neu bearbeitete Auflage*, 6th ed. Weinheim: Wiley-VCH Verlag GmbH & Co. KGaA, 2008.

[5] C. P. Steinmetz, "On the law of hysteresis," *American Institute of Electrical Engineers, Transactions of the*, vol. IX, no. 1, pp. 1–64, Jan 1892.

[6] T. J. E. Miller, *Speed's Electric Motors: An Outline of Some of the Theory in the Speed Software for Electric Machine Design With Problems and Solutions*. Magna Physics, 2004.

[7] J. Willberger, "Ac motor design and evaluation for automotive traction applications," Ph.D. dissertation, Graz University of Technology, 2011.

[8] A. Boglietti, A. Cavagnino, D. Staton, M. Shanel, M. Mueller, and C. Mejuto, "Evolution and modern approaches for thermal analysis of electrical machines," *Industrial Electronics, IEEE Transactions on*, vol. 56, no. 3, pp. 871–882, March 2009.

[9] G. Jiang, L. Diao, and K. Kuang, *Advanced Thermal Management Materials*. New York, Heidelberg, Dordrecht, London: Springer Verlag, 2013.

[10] P. Mellor, D. Roberts, and D. Turner, "Lumped parameter thermal model for electrical machines of TEFC design," *Electric Power Applications, IEE Proceedings B*, vol. 138, no. 5, pp. 205–218, Sep 1991.

[11] UNECE. Working party on pollution and energy (grpe). Accessed on 2014-06-07. [Online]. Available: http://www.unece.org/trans/main/wp29/wp29wgs/wp29grpe/wltp_dhc11.html

[12] EPA. Federal test procedure revisions. Accessed on 2014-06-07. [Online]. Available: http://www.epa.gov/otaq/sftp.htm#cycles

[13] L. Guzzella and A. Amstutz. (2005) The qss toolbox manual. Accessed on 2014-06-07. [Online]. Available: http://www.idsc.ethz.ch/Downloads/DownloadFiles/qss

[14] M. Kamiya, Y. Kawase, T. Kosaka, and N. Matsui, "Temperature distribution analysis of permanent magnet in interior permanent magnet synchronous motor considering pwm carrier harmonics," in *Electrical Machines and Systems, 2007. ICEMS. International Conference on*, 2007, pp. 2023–2027.